Journal of Applied Polymer Science

Effective Thermal Conductivity and Thermal Properties of Phthalonitrile-Terminated Poly(arylene ether nitriles) Composites with Hybrid Functionalized Alumina

Mengdie Liu, Kun Jia, Xiaobo Liu

Research Branch of Functional Materials, Institute of Microelectronic & Solid State Electronic, High-Temperature Resistant Polymers and Composites Key Laboratory of Sichuan Province, University of Electronic Science and Technology of China, Chengdu 610054, People's Republic of China

Correspondence to: K. Jia (E-mail: jiakun@uestc.edu.cn) and X. Liu (E-mail: liuxb@uestc.edu.cn)

ABSTRACT: A polymer-based thermal conductive composite has been developed. It is based on a dispersion of micro- and nanosized alumina (Al_2O_3) in the phthalonitrile-terminated poly (arylene ether nitriles) (PEN-*t*-ph) via solution casting method. The Al_2O_3 with different particle sizes were functionalized with phthalocyanine (Pc) which was used as coupling agent to improve the compatibility of Al_2O_3 and PEN-*t*-ph matrix. The content of microsized functionalized Al_2O_3 (m-*f*-Al_2O_3) maintained at 30 wt % to form the main thermally conductive path in the composites, and the nanosized functionalized Al_2O_3 (n-*f*-Al_2O_3) act as connection role to provide additional channels for the heat flow. The thermal conductivity of the *f*-Al_2O_3/PEN-*t*-ph composites were investigated as a function of n-*f*-Al_2O_3 loading. Also, a remarkable improvement of the thermal conductivity from 0.206 to 0.467 W/mK was achieved at 30 wt % n-*f*-Al_2O_3 loading, which is nearly 2.7-fold higher than that of pure PEN-*t*-ph polymer. Furthermore, the mechanical testing reveals that the tensile strength increased from 99 MPa for pure PEN-*t*-ph to 105 MPa for composites with 30 wt % m-*f*-Al_2O_3 filler loading. In addition, the PEN-*t*-ph composites possess excellent thermal properties with glass transition temperature (T_g) above 184°C, and initial degradation temperature (T_{id}) over 490°C. © 2014 Wiley Periodicals, Inc. J. Appl. Polym. Sci. **2015**, *132*, 41595.

KEYWORDS: composites; properties and characterization; thermal properties

Received 7 August 2014; accepted 3 October 2014

DOI: 10.1002/app.41595

INTRODUCTION

Recently, polymer-based composites with good thermal properties are highly desirable for using in a broad range of potential applications, because these properties are directly related to the performance and service life as well as reliability of various devices, including automobiles, microelectronics, aerospace, and so on. The increased demands of thermally conductive materials have intensified the fundamental studies at nanoscale level to develop filled polymer-based composites with improved thermal performance.[1–8] Alumina (Al_2O_3) has been considered as a reasonable ceramic filler for various purposes because of its favorable thermal conductivity (30–40 W/mK) and low thermal expansion coefficient. The Al_2O_3 also exhibits excellent resistance to oxidation and chemical corrosion.[9–12] However, despite the advantages of Al_2O_3, the poor interfacial interaction between the microsized inorganic filler and organic matrix would limit its utilization in the polymer for high performance applications. Furthermore, the addition of nanoparticles to the polymer matrix will present great challenges because of their extremely small dimensions, large surface area, and high surface energy. Hence, to eliminate the agglomeration of Al_2O_3 particles with different particle sizes and facilitate the particles/matrix interaction, effective method such as surface functionalization was always used to disperse the inorganic particles into polymer matrix.[13–17] In this article, bisphthalonitrile (BPH) and 4, 4′-Diaminediphenyl sulfone (DDS) were selected as organic modifier and curing agent to prepare the surface functionalized Al_2O_3 (*f*-Al_2O_3).

In this article, we combine two different particle sizes of *f*-Al_2O_3 fillers for incorporation into the phthalonitrile-terminated poly (arylene ether nitriles) (PEN-*t*-ph). The PEN-*t*-ph possesses outstanding chemical properties, good thermal stability as well as high mechanical strength.[18–20] Moreover, the nitrile groups on the aromatic rings and the terminal of molecular chain appear to serve as a potential site for polymer cross-linking reaction to form thermally stable phthalocyanine rings. The presence of nitrile groups in PEN-*t*-ph could promote the adhesion of the resin to many substrates by polar interaction with functional groups.

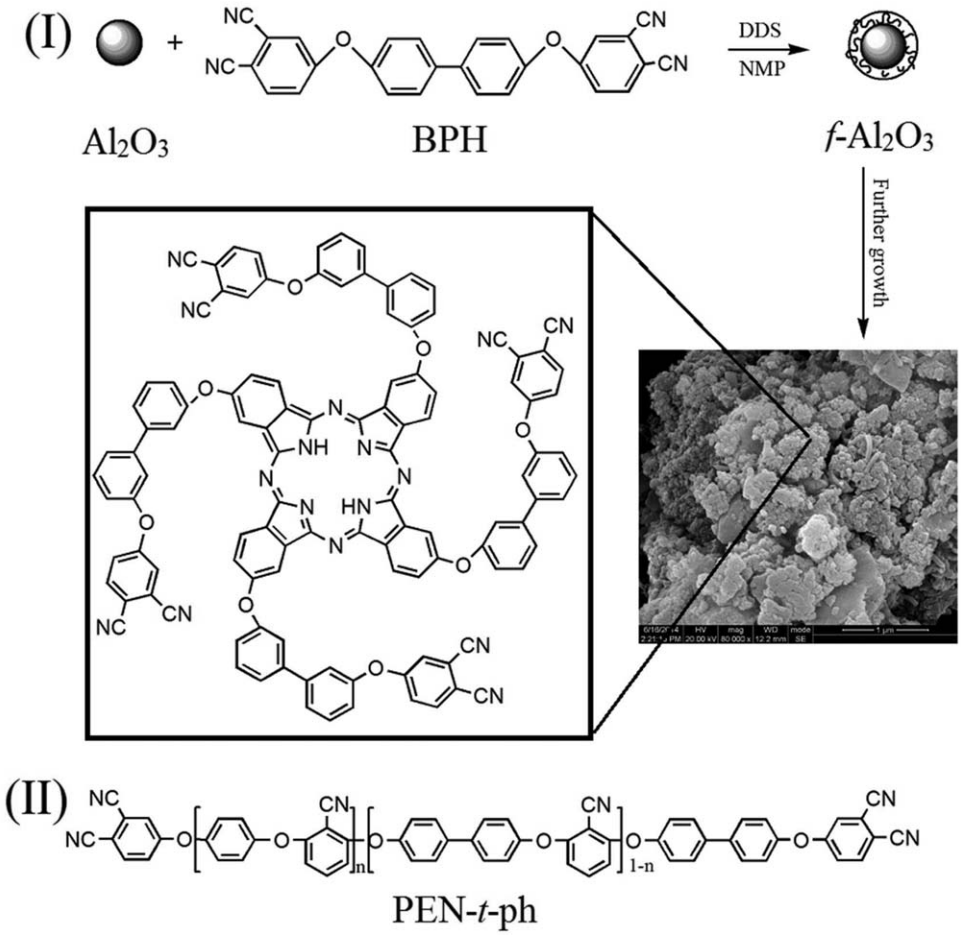

Scheme 1. Illustration of (I) the preparation of *f*-Al_2O_3 and (II) the structure of PEN-*t*-ph.

The idea of using different filler-type mixtures comprised of two or more traditional filler to fabricate the thermally conductive composites has already been explored in the literature.[21–23] There is no doubt that the homogeneous dispersion of thermally conductive filler in the polymer matrix can result in an increase in thermal conductivity of the composites. However, in industrial field, well-balanced composites with enhanced properties and good processability are desired. According to the previous study, the PEN-*t*-ph composites with 30 wt % microsized nitrile functionalized Al_2O_3 exhibits good flexibility to meet the demand of practical application.[17] In this study, the mass fraction of m-*f*-Al_2O_3 was fixed at 30 wt % to obtain composites with enhanced thermal conductivity. Nevertheless, the introduction of individual microsized *f*-Al_2O_3 (m-*f*-Al_2O_3) shows indistinctive improvement on the thermal conductivity of the polymer-based composites. It is due to that the content of m-*f*-Al_2O_3 under 30 wt %, the most conductive particles are encapsulated by the PEN-*t*-ph matrix completely and cannot form a compact packing structure, and a discrete distribution even occur in the polymer composites. Thus, in terms of heat transfer, the interaction between m-*f*-Al_2O_3 is very weak and the surrounding matrix provides the dominant contribution to the thermal flow. Therefore, we are proposing to substitute the polymer matrix by nanosized *f*-Al_2O_3 (n-*f*-Al_2O_3) to fill the resin-rich area between the m-*f*-Al_2O_3 particles. The nanoparticles ranged from 20–30 nm in spherical shapes. The m-*f*-Al_2O_3 formed the main thermally conductive path in the composites, and the n-*f*-Al_2O_3 as the connection role between the larger particles to form conductivity network to obtain high thermal conductivity.

Here, we report the preparation of large-scale *f*-Al_2O_3 and their utilization in the PEN-*t*-ph polymer. The illustration of (I) the preparation of *f*-Al_2O_3 and (II) the structure of PEN-*t*-ph was shown in Scheme 1. Detailed morphological studies and structures of the *f*-Al_2O_3 were carried out. Further property investigations of the novel composites were performed in detail. For the *f*-Al_2O_3/PEN-*t*-ph composites studied, the mass fraction of m-*f*-Al_2O_3 was fixed at 30 wt % in all composites and the loading of n-*f*-Al_2O_3 are varied to study their efficiency in enhancing the thermal conductivity of the composite.

EXPERIMENTAL

Materials

Phthalonitrile-terminated poly (arylene ether nitriles) (PEN-*t*-ph) were synthesized via *4*-nitrophthalonitrile reacting with hydroxyl groups on the terminals of PEN-OH by Union Laboratory of Special Polymers of UESTC-FEIYA, Chengdu, China. Al_2O_3 was purchased from Shanghai Hufeng Chemical Holding, Shanghai, China. Bisphthalonitrile (BPH) was

synthesized (melting point: 134°C) in our laboratory.[24] 4, 4′-Diaminediphenyl sulfone (DDS, as curing agent) was purchased from Sichuan Dongcai chemicals. *N*-Methyl-*2*-pyrrolidone (NMP) was purchased from Tianjin Bodi Chemical Holding, Tianjin, China. All the reagents were used without further purification.

Preparation of Functionalized Al_2O_3

The synthesis of functionalized Al_2O_3 was carried out as follows. First, 5.0 g pristine Al_2O_3 particles were added into a certain amount of NMP solvent and treated with violent ultrasonic waves (ultrasonic frequency: 80 kHz, electric power: 200 W) at room temperature for 0.5 h. Meanwhile, 5.0 g BPH and 10.0 mL NMP were mixed in a 50-mL three-necked round-bottom flask equipped with mechanical stirrer and refluxing condenser. The mixture was heated for 30 min to dissolve sufficiently. After then, Al_2O_3 suspension and 0.1 g DDS were slowly added to the bottle, and the mixture was refluxed at 200°C for 6 h. The product was obtained by centrifugation and washed with distilled water for several times and finally dried at 80°C overnight. The pure phthalocyanine (Pc) was prepared as comparison in the same condition.

Preparation of *f*-Al_2O_3/PEN-*t*-ph Composites

The preparation of *f*-Al_2O_3 was carried out according to previous literatures.[25] In a typical experimental procedure, the *f*-Al_2O_3/PEN-*t*-ph composites were obtained via solution casting method with continuous ultrasonic dispersion technology. Subsequently, further hot pressure casting technique was used to facilitate the cross-linking reaction of nitrile groups on the PEN-*t*-ph matrix and Pc. The preparation of PEN-*t*-ph/*f*-Al_2O_3 was generally as follows. First, a weight-measured of n-*f*-Al_2O_3 and m-*f*-Al_2O_3 were added in a certain amount NMP solvent to form suspension by violent ultrasonic waves (ultrasonic frequency: 80 kHz, electric power: 200 W) for 30 min. The mass fraction of m-*f*-Al_2O_3 was fixed at 30 wt %. The mass fraction of n-*f*-Al_2O_3 was fixed at 0, 5, 10, 15, 20, and 30 wt %, respectively. At the same time, certain content of PEN-*t*-ph was dissolved sufficiently in 15 mL NMP solvent with mechanical stirring. Then, the suspension of mixed *f*-Al_2O_3 was slowly added into the PEN-*t*-ph solution. The mixture was refluxed at 200°C with a mechanical stirring for 30 min to ensure that the particles were well dispersed in the PEN-*t*-ph matrix. After then the mixture was treated with ultrasonic for another 30 min to obtain more stable and uniform suspension. Finally, the mixture was then casted onto a clean and horizontal glass plate and dried in an oven at temperature of 80, 100, 140, 160, and 200°C for 1 h, respectively, to remove the solvent. After cooling naturally to room temperature, the PEN-*t*-ph composite films were obtained.

Afterwards, the films were crushed into small pieces and subsequently filled in the template with size about 15 cm × 5 cm and a thickness of approximately 0.4 mm which was prepared in advance. And then, the films were treated with hot pressure casting technique at 320°C for 2 h along with the pressure maintained at 10 MPa. As a reference, cross-linked composites filled with different contents of *f*-Al_2O_3 particles were obtained in the same condition. Pure PEN-*t*-ph without filler has also been prepared for comparison. The contents of the n-*f*-Al_2O_3 are 0, 5, 10, 15, 20, and 30 wt %. Corresponding to the different contents of n-*f*-Al_2O_3, the composites were named as C1–C6, respectively.

Characterizations

The morphologies of functionalized Al_2O_3 and fracture surfaces of the composites were observed by a JEOL JSM-5900LV scanning electron microscopy (SEM). FTIR spectra were recorded with Shimadzu FTIR8400S Fourier Transform Infrared Spectrometer in KBr pellets in air. UV–vis spectra were recored on a UV2501-PC spectrophotometer. The thermal conductivity measurements of the obtained composites were performed on a Netzsch LFA 447 instrument (Xenon NanoFlash). The measurements were conducted at room temperature, and each sample was measured three times to ensure equilibrium of sample temperature. Differential scanning calorimetry (DSC) analyses were performed on TA Instrument DSC Q100 modulated thermal analyzer under nitrogen atmosphere with a flow rate of 50 mL/min at a heating rate 10°C/min from room temperature to 350°C. Thermal gravimetric analyses (TGA) of the composites were carried out on a TA Instruments TGA Q50 under nitrogen purge of 60 mL/min at a heating rate 20°C/min from 50 to 800°C. The mechanical properties of the composites were measured with a SANS CMT6104 Series Desktop Electromechanical Universal Testing Machine with sample size of about 10 mm × 120 mm, and gained as average values for every four samples.

RESULTS AND DISCUSSION

Characterization of *f*-Al_2O_3

The morphology and chemical structure of the synthesized *f*-Al_2O_3 were characterized by SEM, FTIR, UV–vis and TGA. The uniform distribution of Pc on the *f*-Al_2O_3 was examined by SEM as shown in Figure 1. Figure 1(a,c) exhibit the typical SEM images for n-*f*-Al_2O_3 and pristine n-Al_2O_3, respectively. It could be observed that the surface of the n-*f*-Al_2O_3 is coarser than pristine n-Al_2O_3, which is due to the fact that the Pc was randomly dispersed on Al_2O_3 surface. As shown in Figure 1(b,d), the microsized Al_2O_3 demonstrate irregular shape with particle size at the micrometer sizes in the range of hundreds of nanometers. The surface of pristine m-Al_2O_3 is quite smooth. After chemical and physical treatments during the functionalization process, the surface of Al_2O_3 tends to be tough, which is beneficial to improve their dispersibility and compatibility in polymer matrix.

To further verify the Pc on the surface of *f*-Al_2O_3, the as-prepared *f*-Al_2O_3 particles were confirmed by FTIR and UV–vis spectra. Figure 2 shows FTIR spectra for the pristine m-Al_2O_3 (curve **a**), n-*f*-Al_2O_3 (curve **b**), and m-*f*-Al_2O_3 (curve **c**). The characteristic absorption band of pure Pc was observed from curve **d**. As can be seen, the absorption band of nitrile group at 2230 cm^{-1} was clearly observed, suggests the presence of nitrile functional groups on the Al_2O_3.[26] Besides, the absorption band at 1250 cm^{-1} was characteristic of aromatic ether group. The characteristic absorption band at 1590 cm^{-1} was attributed to N—H stretching. Moreover, the particular characteristic band at 1490 cm^{-1} was assigned to the —C=N—.[27] Another feature should be noted is that the peak at 1010 cm^{-1} was assigned to the stretching vibration of phthalocyanine ring.[28] Furthermore,

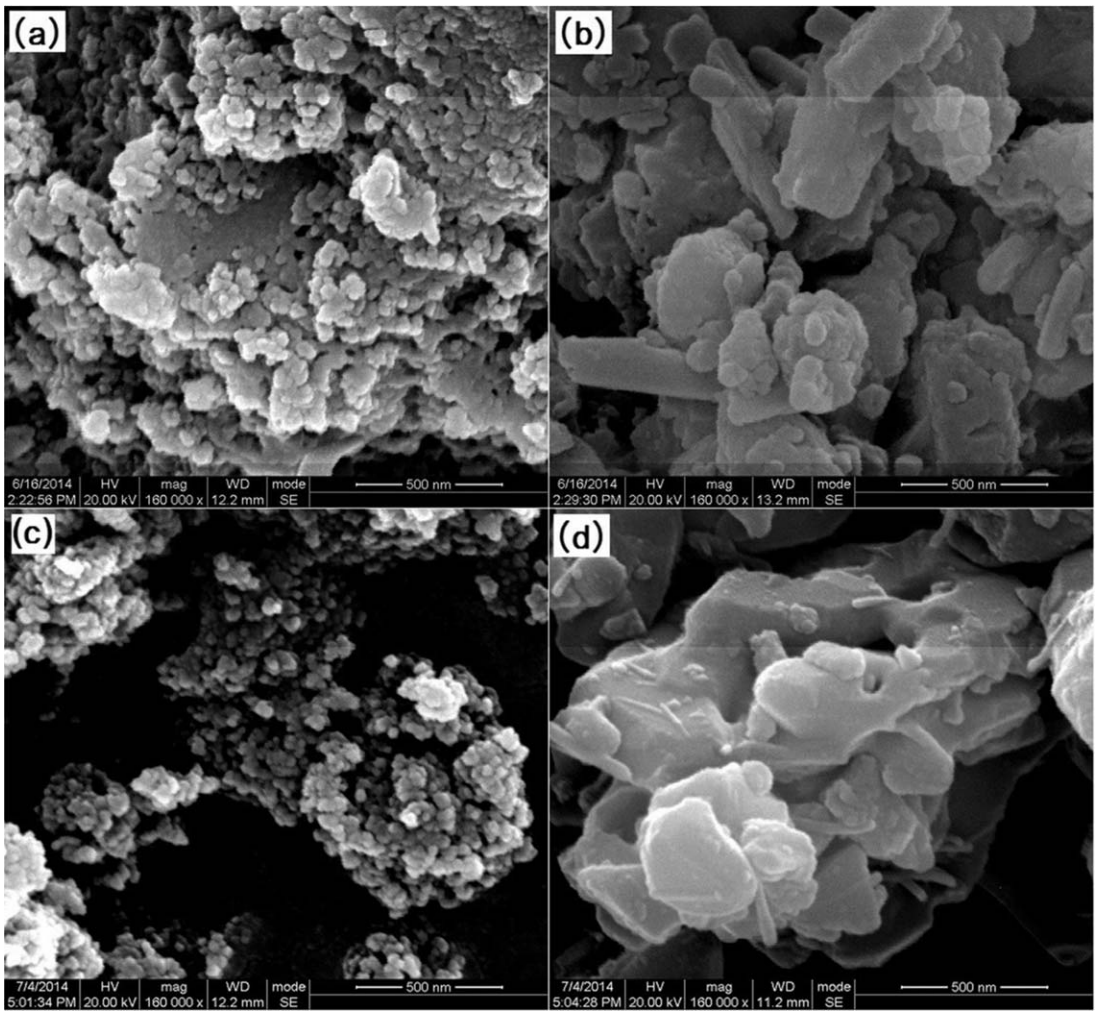

Figure 1. SEM images of surface functionalized Al_2O_3: (a) n-*f*-Al_2O_3, (b) m-*f*-Al_2O_3, (c) pristine n-Al_2O_3, and (d) pristine m-Al_2O_3.

the broad absorption band in the wavenumber range from 500 to 900 cm^{-1} is characteristic of the amorphous nano- and micro-Al_2O_3 powder. Apart from the IR analysis, the as-prepared *f*-Al_2O_3 particles were also characterized by UV–vis spectra. The two spectra were recorded for an equal concentration of each sample (Figure 3). The characteristic absorption

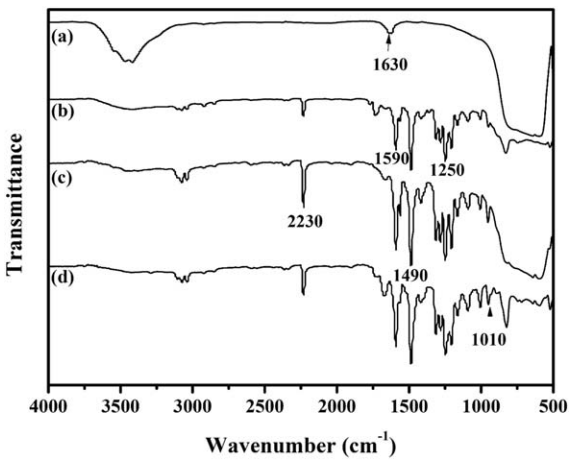

Figure 2. FTIR spectra of (a) m-Al_2O_3, (b) n-*f*-Al_2O_3, (c) m-*f*-Al_2O_3, and (d) pure Pc.

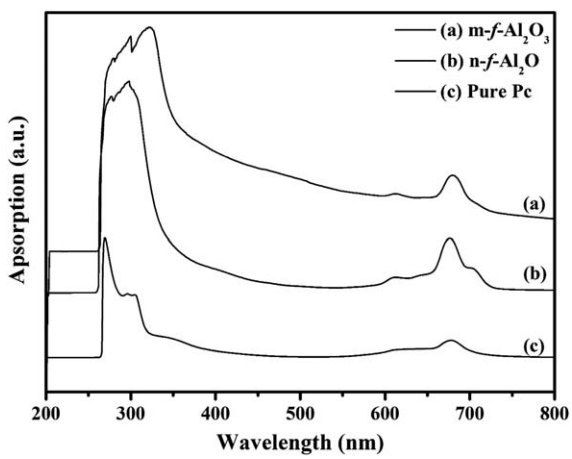

Figure 3. UV–vis spectra of (a) m-*f*-Al2O3, (b) n-*f*-Al2O3, and (c) pure Pc.

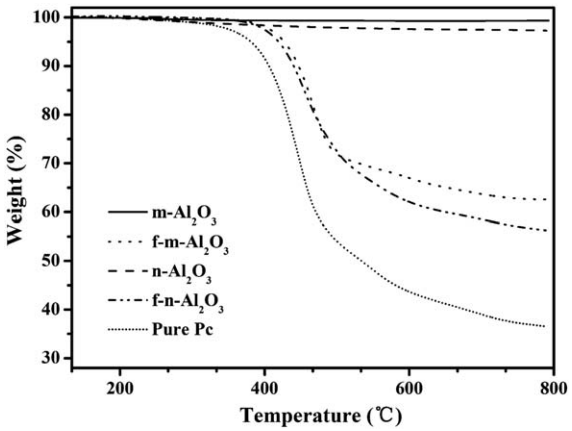

Figure 4. TGA curves of pristine Al_2O_3, surface functionalization Al_2O_3, and pure Pc.

band of pure Pc to distinguish from functionalized Al_2O_3 was observed from curve **c**. It is shown that *f*-Al_2O_3 exhibit two obvious absorption bands centered at 250–450 nm and 550–729 nm. The absorption peaks at 676 and 609 nm are characteristic Q-band absorption bands of phthalocyanine, corresponding to the $\pi \rightarrow \pi^*$ transition of the sample from the HOME to the LUMO of Pc^{2-} ring. In addition, the other band centered at 250–450 nm should belong to the B-band absorption of Pc. These results demonstrated that the Pc has successfully formed on the surface of Al_2O_3, which are consistent with the results of SEM and FTIR.

Apart from the aforementioned analysis, TGA was used to further calculate the content of Pc on the surface of Al_2O_3. Figure 4 shows the TGA curves of pristine Al_2O_3, *f*-Al_2O_3, and pure Pc in nitrogen. It is obvious that the weigt of pristine Al_2O_3 does not lose in the testing temperature. And the curves show that the weight of n-*f*-Al_2O_3 and m-*f*-Al_2O_3 lose 43.7 wt % and 37.4 wt % respectively, which is attributed to the decomposition of the introduced Pc oligomer chains. Meanwhile, the char yield of the pure Pc was 36.6 wt % when the temperature reached 800°C. Thus, about 68.9 and 59.0 wt % organic Pc has been incorporated into the nanosized Al_2O_3 and microsized Al_2O_3, respectively. The Pc content on the surface of Al_2O_3 was calculated by

$$\omega_{Pc}(\%) = \frac{1-\omega_1}{1-\omega_2} \times 100\%$$

where ω_1 and ω_2 are the char yield of the *f*-Al_2O_3 and pure Pc, respectively.

It can be observed that the content of Pc on the n-*f*-Al_2O_3 is higher than that on microsized Al_2O_3, which might be due to the fact that nanosized Al_2O_3 provided certain specific surface area and endow high functionalization efficiency. Besides, it is noteworthy that the initial degradation temperature (T_{id}) of the *f*-Al_2O_3 is up to 420°C, indicating that the filler possess high thermal stability, which is a prerequisite to ensure good thermal stability of the composite.

Morphological Properties of *f*-Al_2O_3/PEN-*t*-ph Composites

It is well known that the good compatibility between filler and polymer matrix could result in excellent mechanical properties and high performance.[29–32] Figure 5 shows the morphologies of fractured surfaces of the pure PEN-*t*-ph polymer, *f*-Al_2O_3/PEN-*t*-ph composites C1 and C6, respectively. It is noted that the pure PEN-*t*-ph polymer exhibits a homogeneous continuous phase and the fractured surface is rather smooth and glassy. Compared to the pure polymer, the morphology of C1 composite displays a well visual distribution, which attributed to the uniform dispersion of m-*f*-Al_2O_3 filler in the PEN-*t*-ph matrix without any aggregation. In addition, it can be observed that the m-*f*-Al_2O_3 particles are encapsulated by the PEN-*t*-ph matrix completely. The results indicate that there is a strong interfacial bonding between *f*-Al_2O_3 and PEN-*t*-ph matrix, indicating the effective surface functionalization of Al_2O_3 particles in this study. In comparison with the uniform distribution observed from C1 composites in Figure 5(b), the fractured surfaces of C6 composites with 30 wt % n-*f*-Al_2O_3 was shown in Figure 5(c). It can be observed that the image exhibits complex structures with larger m-*f*-Al_2O_3 particles surrounding by massive n-*f*-Al_2O_3 to form conductive bridge, which could result in significantly improvement of thermal conductivity. However, the sample at higher filler concentration may result in aggregation to some extent. These excessive conductivity particles may act as crazes in the composites and consequently be sites for microcracks.

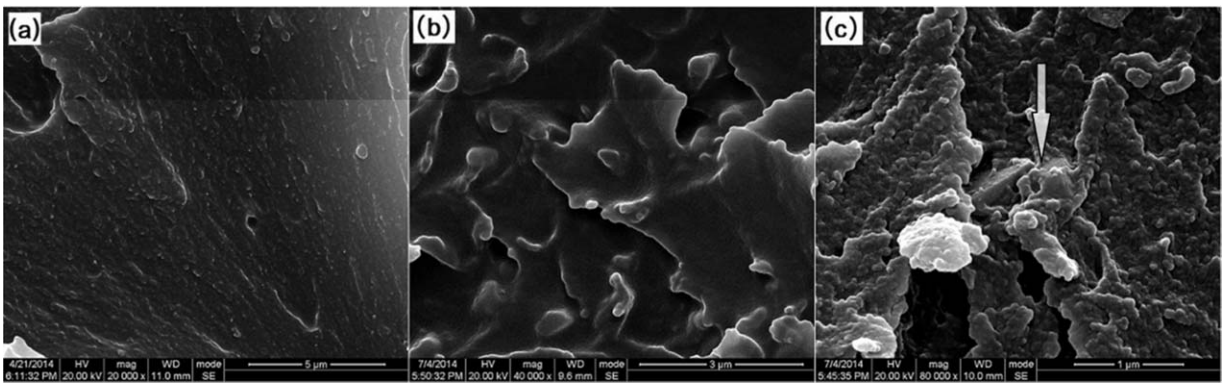

Figure 5. SEM images of (a) pure polymer and the *f*-Al_2O_3/PEN-*t*-ph composites with (b) 0 wt % n-*f*-Al_2O_3 content, (c) 30 wt % n-*f*-Al_2O_3 content.

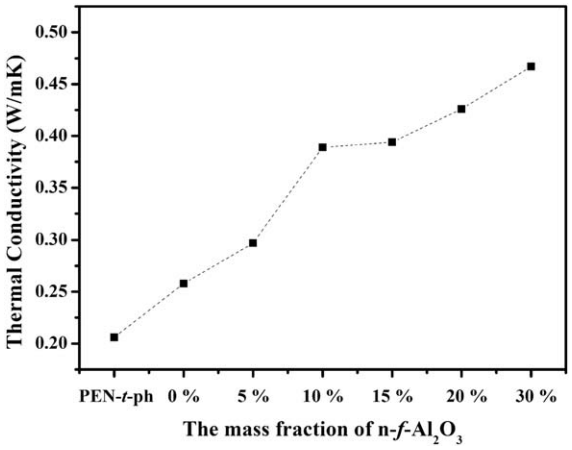

Figure 6. Thermal conductivity of the f-Al_2O_3/PEN-t-ph composites as a function of n-f-Al_2O_3 loading.

Thermal Conductivity of f-Al_2O_3/PEN-t-ph Composites

Figure 6 shows the through-plane thermal conductivity of the composites as a function of n-f-Al_2O_3 loading with the m-f-Al_2O_3 content maintained at 30 wt %. The pure polymer revealed a thermal conductivity value of 0.206 W/mK. However, the thermal conductivity of the composite with 30 wt % m-f-Al_2O_3 loading is only 0.258 W/mK, which indicated that the larger particles occurs in the polymer composites in the form of "island" as shown in Figure 5(b). With the incorporation of n-f-Al_2O_3, it is clear that the thermal conductivity increased rapidly with the increase of n-f-Al_2O_3 loading, which would reduce the thickness of thermally insulating PEN-t-ph matrix between adjacent m-f-Al_2O_3 and facilitate the formation of a random thermally conductive bridge or network.[33] The f-Al_2O_3/PEN-t-ph composites with 30 wt % n-f-Al_2O_3 gave thermal conductivity of 0.467 W/mK, which is nearly 1.81-fold higher than that of C1 composite. Thus the combination of nano- and microsized f-Al_2O_3 demonstrates a strong synergistic effect to obtain high thermal conductivity than individual filler.

Mechanical Properties of f-Al_2O_3/PEN-t-ph Composites

Mechanical properties are an important indicator in measuring the strength of material to ensure practical applications. In this article, mechanical tests were performed to evaluate the effect of n-f-Al_2O_3 on the mechanical properties of f-Al_2O_3/PEN-t-ph composites. As shown in Figure 7, the tensile strength increases from 99 MPa for pure PEN-t-ph to 105 MPa for C1 composites. Furthermore, the tensile modulus of all samples increases from 2179 to 3520 MPa along with increasing m-f-Al_2O_3 loading. The reinforcement is attributed to the enhanced interfacial compatibility between the functionalized Al_2O_3 and polymer matrix. Meanwhile, the nitrile groups exist in the surface of the functionalized Al_2O_3 appears to serve as a potential site to form a cross-linked network structure, and thus limited the cleavage of polymer chains in the stretching process. However, with the increase of n-f-Al_2O_3 loading, the tensile strength decreased gradually, which might be due to the agglomeration of f-Al_2O_3 in the PEN-t-ph matrix. The excessive filler acts as defects in

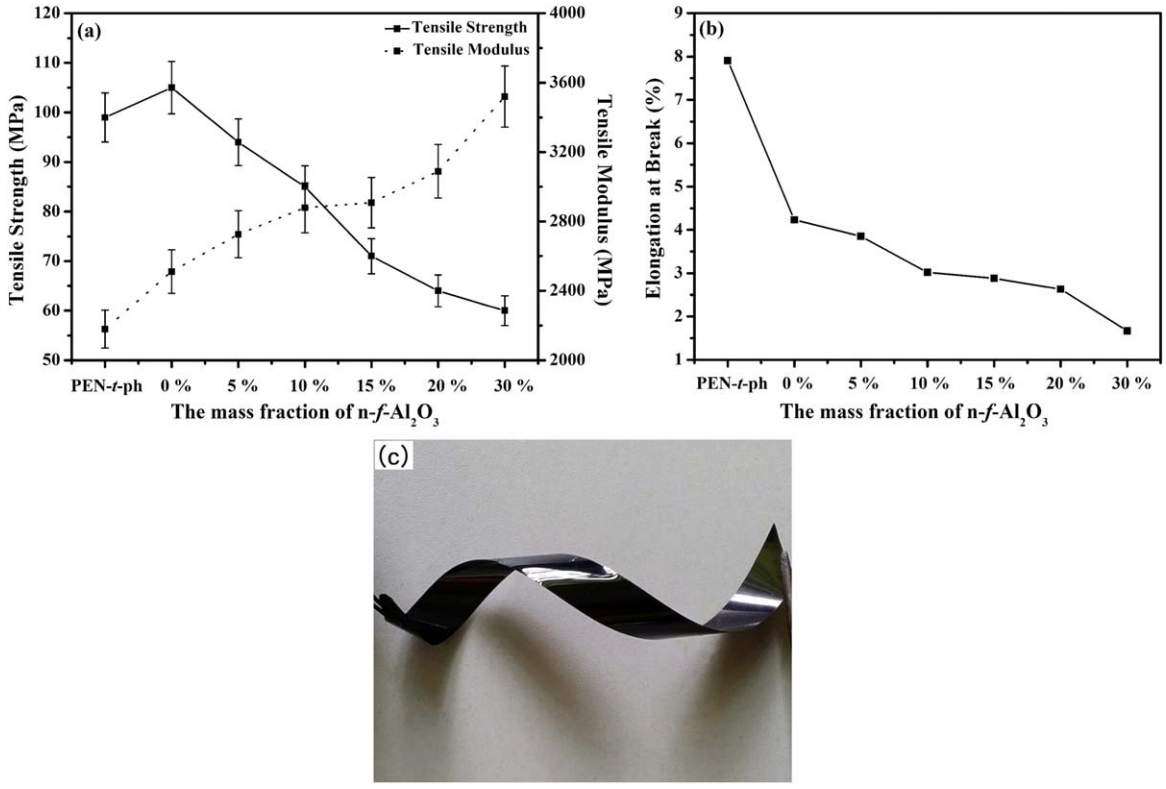

Figure 7. Mechanical properties of the f-Al_2O_3/PEN-t-ph composites: (a) tensile strength and tensile modulus, (b) elongation at break, (c) digital photo of f-Al_2O_3/PEN-t-ph composite with 30 wt % n-f-Al_2O_3. [Color figure can be viewed in the online issue, which is available at wileyonlinelibrary.com.]

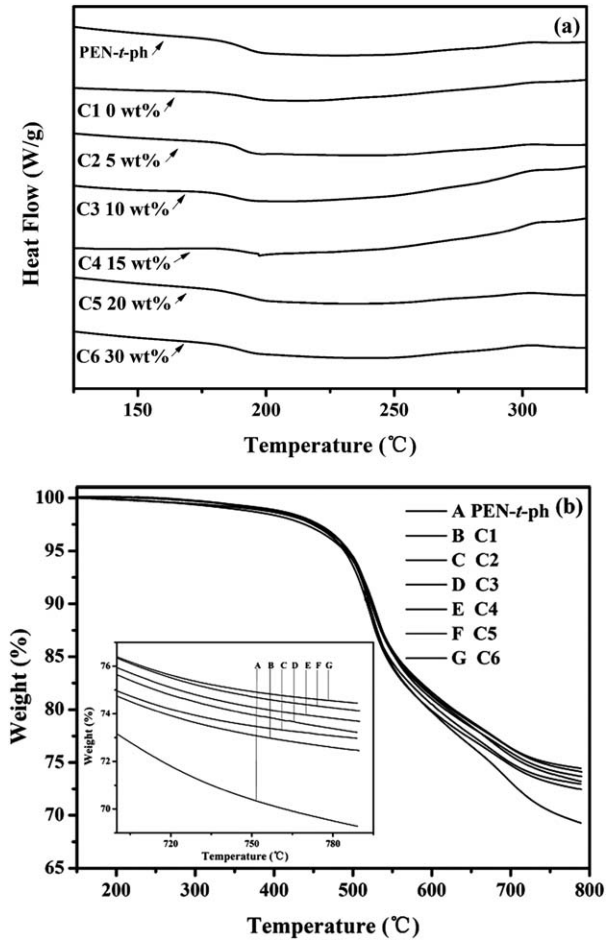

Figure 8. DSC (a) and TGA (b) curves of the *f*-Al_2O_3/PEN-*t*-ph composites with various contents of n-*f*-Al_2O_3.

the composites and consequently be sites for microcracks, which is according with the SEM observation. On the other hand, the massive *f*-Al_2O_3 cannot be conglutinated entirely by the polymer matrix and causes a decrease on specific surface of the particles in the composites, thus the applied stress cannot transfer from the matrix to the *f*-Al_2O_3 filler efficiently as expected. Besides, the elongation at break of the *f*-Al_2O_3/PEN-*t*-ph composites significant decreased with increasing *f*-Al_2O_3 loading. The decrease in elongation at break indicates that the addition of *f*-Al_2O_3 restricts the molecular chain movement of the polymer. In addition, the stress concentration and microcracks may also result in the material deformation focused on the small zone and affect the elongation at break of the composites. In addition, Figure 7(c) demonstrates the high performance of flexibility of C6 composite thin film even with 30 wt % nano- and microsized *f*-Al_2O_3 loading, which indicated that the composites exhibit enhanced thermal conductivity with flexibility maintained.

Thermal Properties of *f*-Al_2O_3/PEN-*t*-ph Composites

The DSC and TGA were plotted to investigate the thermal stability and decomposition behavior of the pure PEN-*t*-ph and *f*-Al_2O_3/PEN-*t*-ph composites as a function of the n-*f*-Al_2O_3 contents. Figure 8(a,b) shows DSC and TGA curves of pure PEN-*t*-ph and composites with various content of n-*f*-Al_2O_3 under a nitrogen atmosphere. The glass transition temperature (T_g), initial degradation temperature (T_{id}), and maximum decomposition rate temperature (T_{max}) of the composites are summarized in Table I. As can be seen from Figure 8(a), the T_g of the pure polymer was observed at 184°C. With the addition of *f*-Al_2O_3, the T_g of the composites range from 185 to 192°C, indicating that the *f*-Al_2O_3/PEN-*t*-ph composites possess high working temperature in engineering applications. The improvements in T_g of the samples with the presence of *f*-Al_2O_3 might attributed to the addition of hybrid filler, which restricted the segmental motions of the polymer macromolecules to some extent.

These effects also decrease the interfacial thermal resistance between the filler and PEN-*t*-ph matrix, leading to increased thermal conductivity of the composites. From the TGA curves [Figure 8(b)], it can be observed that all the composites exhibit almost the same decomposition behavior as pure PEN-*t*-ph except the slightly difference in char yield. As shown in Table I, the T_{id} of all samples are ranging from 489 to 495°C, indicating the excellent thermal stability of PEN-*t*-ph composites. In addition, the data listed in Table I reveals that all the composites with T_{max} ranging of 523°C ± 5°C, which might be owing to the rapid decomposition of macromolecular chain. In conclusion, all the nanocomposites show high thermal stability which is mainly attributed to the outstanding thermal property of PEN-*t*-ph matrix.

CONCLUSION

In summary, an efficient approach to fabricate the functionalized Al_2O_3 with Pc was successfully demonstrated, which was confirmed by scanning electron microscopy (SEM), fourier transform infrared (FTIR), UV–vis spectroscopy, and thermogravimetric analysis (TGA). The *f*-Al_2O_3 with different shape and size were used in combination to obtain novel polymer composites by solution blending method and further hot pressure casting technique. The content of m-*f*-Al_2O_3 is maintained at 30 wt %, and the effects on the properties of *f*-Al_2O_3/PEN-*t*-ph composites were evaluated as a function of n-*f*-Al_2O_3 content. SEM images indicate that the composites with 30 wt % n-*f*-Al_2O_3 exhibit complex morphology with larger m-*f*-Al_2O_3 particles surrounding by massive n-*f*-Al_2O_3 to form conductive bridge,

Table I. Thermal Properties of Pure PEN-*t*-ph and *f*-Al_2O_3/PEN-*t*-ph Composites

Sample	PEN-t-ph	C1	C2	C3	C4	C5	C6
T_g (°C)	184	185	186	186	191	192	190
T_{id} (°C)	494	493	489	491	490	495	495
T_{max} (°C)	523	518	519	524	529	524	522

which corresponds to the maximum value of 0.467 W/mK observed in thermal conductivity. Furthermore, the mechanical test demonstrates the composites possess excellent flexibility. Furthermore, the DSC and TGA results reveal that the T_g of the composites is above 185°C and the T_{id} is as high as 495°C, indicating that the composites with various content of *f*-Al_2O_3 maintain the excellent thermal stability. This study demonstrates a new route to obtain the comprehensive performances of PEN-*t*-ph composites, which will greatly promote their potential industrial application.

ACKNOWLEDGMENTS

We thank for financial support of this work from the National Natural Science Foundation (Nos. 51173021, 51373028) and "863" National Major Program of High Technology (2012AA03A212).

REFERENCES

1. Yan, H.; Kou, K. J. *Mater. Sci.* **2014**, *49*, 1222.
2. Moisala, A.; Li, Q.; Kinloch, I. A.; Windle, A. H. *Compos. Sci. Technol.* **2006**, *66*, 1285.
3. Wong, C. P.; Bollampally, R. S. *J. Appl. Polym. Sci.* **1999**, *74*, 3396.
4. Ganguli, S.; Roy, A. K.; Anderson, D. P. *Carbon* **2008**, *46*, 806.
5. Kumlutaş, D.; Tavman, I. H.; Çoban, T. M. *Compos. Sci. Technol.* **2003**, *63*, 113.
6. Garrett, K. W.; Rosenberg, H. M. *J. Phys. D: Appl. Phys.* **1974**, *7*, 1247.
7. Wurm, A.; Lellinger, D.; Minakov, A. A. *Polymer* **2014**, *55*, 2220.
8. He, H.; Fu, R.; Han, Y. *J. Mater. Sci.* **2007**, *42*, 6749.
9. Xie, H.; Wang, J.; Xi, T. *J. Appl. Phys.* **2002**, *91*, 4568.
10. McGrath, L. M.; Parnas, R. S.; King, S. H. *Polymer* **2008**, *49*, 999.
11. Sim, L. C.; Lee, C. K.; Ramanan, S. R. *Polym-Plast. Technol.* **2006**, *45*, 301.
12. Adhikari, R.; Henning, S.; Lebek, W. *Macromol. Sympos.* **2005**, *231*, 116.
13. Bartholome, C.; Miaudet, P.; Derré, A. *Compos. Sci. Technol.* **2008**, *68*, 2568.
14. Sun, L.; Warren, G. L.; O'reilly, J. Y. *Carbon* **2008**, *46*, 320.
15. KumaráThakur, V.; JináTan, E.; SeeáLee, P. *RSC. Adv.* **2011**, *1*, 576.
16. Nakaramontri, Y.; Kummerlöwe, C.; Nakason, C. *Polym. Compos.* **2014**. DOI: 10.1002/pc.23122.
17. Liu, M. D.; Xu, M.; Tong, L. *J. Polym. Res.* **2014**, *21*, 1.
18. Yang, X.; Zhan, Y.; Yang, J. *Polym. Inter.* **2012**, *61*, 880.
19. Zou, Y.; Liu, X. *J. Appl. Polym. Sci.* **2013**, *129*, 130.
20. Liu, M. D.; Xu, M.; Liu, X. *Polym. Compos.* **2014**. DOI: 10.1002/pc.23131.
21. Lee, G. W.; Park, M.; Kim, J. *Compos. Part A: Appl. Sci.* **2006**, *37*, 727.
22. Yu, A.; Ramesh, P.; Sun, X. *Adv. Mater.* **2008**, *20*, 4740.
23. Hong, J.; Choi, H. S.; Lee, K. S. *Polym. Int.* **2012**, *61*, 639.
24. Tong, L.; Pu, Z.; Huang, X. *J. Appl. Polym. Sci.* **2013**, *130*, 1363.
25. Wang, Z.; Yang, X.; Xu, M. *J. Mater. Sci-Mater. El.* **2013**, *24*, 2610.
26. Yang, X.; Lei, Y.; Zhong, J. *J. Appl. Polym. Sci.* **2011**, *119*, 882.
27. Seoudi, R.; El-Bahy, G. S.; Sayed, Z. A. *J. Mol. Struct.* **2005**, *753*, 119.
28. Zou, Y. K.; Liu, X. B. *J. Appl. Polym. Sci.* **2012**, *125*, 3829.
29. Dang, Z. M.; Wang, H. Y.; Xu, H. P. *Appl. Phys. Lett.* **2006**, *89*, 112902.
30. Shi, D.; Wang, S. X.; Van Ooij, W. J. *Appl. Phys. Lett.* **2001**, *78*, 1243.
31. Sato, K.; Horibe, H.; Shirai, T. J. *Mater. Chem.* **2010**, *20*, 2749.
32. Li, S. Q.; Wang, F.; Wang, Y. J. *Mater. Sci.* **2008**, *43*, 2653.
33. Im, H.; Kim, J. *Carbon* **2012**, *50*, 5429.